Fermi National Accelerator Laboratory

FERMILAB-Conf-98/043

A New MARS and its Applications

O.E. Krivosheev and N.V. Mokhov

Fermi National Accelerator Laboratory
P.O. Box 500, Batavia, Illinois 60510

January 1998

Published Proceedings of the *Third Workshop on Simulating Accelerator Radiation Environments (SARE3)*, KEK, Tsukuba, Japan, May 7-9, 1997

Operated by Universities Research Association Inc. under Contract No. DE-AC02-76CH03000 with the United States Department of Energy

Disclaimer

This report was prepared as an account of work sponsored by an agency of the United States Government. Neither the United States Government nor any agency thereof, nor any of their employees, makes any warranty, expressed or implied, or assumes any legal liability or responsibility for the accuracy, completeness, or usefulness of any information, apparatus, product, or process disclosed, or represents that its use would not infringe privately owned rights. Reference herein to any specific commercial product, process, or service by trade name, trademark, manufacturer, or otherwise, does not necessarily constitute or imply its endorsement, recommendation, or favoring by the United States Government or any agency thereof. The views and opinions of authors expressed herein do not necessarily state or reflect those of the United States Government or any agency thereof.

Distribution

Approved for public release; further dissemination unlimited.

A New MARS and its Applications*

O. E. Krivosheev and N. V. Mokhov

Fermi National Accelerator Laboratory

P.O. Box 500, Batavia, Illinois 60510

January 30, 1998

Abstract

This paper describes MARS14(98) – the newest version of the MARS Monte Carlo code system for fast simulation of hadronic and electromagnetic cascades in shielding, accelerator and detector components in the energy range from a fraction of an electronvolt up to 30 TeV. The main changes compared to the previous release, MARS13, concern the hadron production model tuned with evaluated data and the DPMJET-II code, improved photo- and electro-production of hadrons and muons, improved algorithms for the 3-body decays, particle tracking in magnetic fields, synchrotron radiation by electrons and muons, significantly extended histograming capabilities and material description, and improved computational performance. In addition to direct energy deposition calculations, a new set of fluence-to-dose conversion factors for all particles including neutrino are built into the code. The MARS14(98) system includes links to the MCNP code for neutron transport below 20 MeV, to the ANSYS code for thermal and stress analyses and to the STRUCT code for multi-turn particle tracking in large synchrotrons and collider rings.

1 Introduction

The MARS Monte Carlo code system, being developed over 24 years, allows fast inclusive simulation of three-dimensional hadronic and electromagnetic cascades in shielding, accelerator and detector components in the energy range from a fraction of an electronvolt up to 30 TeV. The code has undergone substantial improvements since the previous documented release, MARS13(95) [1]. The developments were induced by numerous challenging applications (Fermilab accelerator and detector upgrades, LHC machine and detector studies, a 2×2 TeV $\mu^+\mu^-$ collider) as well as

*Submitted to *Proceedings of the Third Workshop on Simulating Accelerator Radiation Environments (SARE3)*, KEK, Tsukuba, Japan, May 7-9, 1997

by a continuous desire to increase code reliability, flexibility and user friendliness. The main changes and new features of the current MARS14 code are described in this paper with several typical examples.

2 Physics, Tracking and Tallies

The main changes in the physics model, tallies, analysis and computing compared to MARS13(95) [1] are listed briefly below.

Cross Sections. Hadron-nucleus elastic and inelastic cross-section description at 10 MeV<E<5 GeV has been updated using data and the systematics [2]. Total photon-nucleus cross sections are extracted from experimental data [3].

Event Generator. Hadron-nucleus event generator at 1 GeV<E<10 TeV has been re-adjusted using evaluated experimental data, a new phenomenological model [4] and the DPMJET-II code [5] with special attention to intermediate energies, high-p_t events, π^0 production and kaon production. An optional use of the DPMJET-II code as an event generator is included. Photon-nucleus hadroproduction is extended to light nuclei [3]. Neutrino-nucleus [6] and deuteron-nucleus [7] event generators are included. The formulae [8] are used to simulate elastic hadron-nucleus scattering at 15 MeV<E<5 GeV, and weight windows are introduced in each inclusive generator.

Muon Production. Simulation algorithms for $\pi^{\pm}\rightarrow\mu^{\pm}\nu(\tilde{\nu})$ and $K^{\pm}\rightarrow\mu^{\pm}\nu(\tilde{\nu})$ decays and for prompt muon production (single muons in charmed meson decays, $\mu^+\mu^-$ pairs in vector muon decays, and the dimuon continuum) with forced generation of weighted muons have been improved. Prompt muons produced in electromagnetic showers are described in detail. Bethe-Heitler pairs $\gamma Z\rightarrow Z\mu^+\mu^-$ are produced at $E_\gamma \geq 0.25$ GeV at a rate of $(m_e/m_\mu)^2$ times that for e^+e^- with the appropriate statistical weights and a complete simulation of electromagnetic showers. It was shown [9] that this approach produces remarkable results that agree with those based on the numerical integration in the Tsai formalism [10]. At $E \geq 45$ GeV direct positron annihilation $e^+e^-\rightarrow\mu^+\mu^-$ is simulated according to [11] with σ=86.8/s nb, where s is in GeV^2, and with $(1+cos^2\theta)$ as the angular distribution.

$\mu\rightarrow e\nu\tilde{\nu}$ **Decays.** Vector momenta of the emitted electrons and neutrinos are sampled according to the differential decay probability of the *Vector–Axial* model of four-fermion interactions [11].

Tracking. Minimal cell linear size, where magnetic field, multiple Coulomb scattering and other "*continuous*" processes are taken into account, is reduced to 0.0001/ρ cm, where ρ is material density in g/cm^3. The descriptions of π^- capture and π^+ decay at rest have been improved. Generation and transport of de-excitation photons are also improved. Undesirable fluctuations in the inclusive description of electromagnetic showers are reduced. Low-energy neutron transport has been replaced with one based on the MCNP4A code as described in Section 4.

Tallies. MARS native and HBOOK-based histograming and analyses have been extended. Dose equivalent scoring based on the ICRP51 flux-to-dose conversion coefficients [12] has been included in addition to direct energy deposition and dose calculations. Detailed scoring of surface current, flux, dose equivalent, particle spectra and time distributions have been added to MARS in addition to track length and collision type estimations of the above tallies in cells. Interface to ANSYS allows detailed thermal and stress analyses (see Section 5). Non-analog scoring of probabilities rather than direct contributions for particle flux and spectra, star density and dose equivalent has been refined.

Visualization. The MARS14 visualization of geometry in solid and wire-frame representations, and of particle tracks and verticies is done with the OpenGL™-based module [13].

Tagging. Geometry and phase-space tagging options, used intensively in studies with MARS (see, e. g., [14, 15, 16]), have been further improved. These allow very efficient way to study a source term, for example.

Computing. Many of the MARS algorithm computing efficiencies have been improved. The code has been modified to run completely in the IEEE-754 double precision mode [17], except for the CERN HBOOK package.

3 Recent Calculations

A few examples of the recent studies with the MARS code are given in Figs. 1–6. Figs. 1 and 2 show pion differential cross-sections on copper and gold nuclei for 14.6 GeV/c protons as calculated with the MARS, DPMJET-II [5] and ARC [18] codes and measured in the E-802 experiment at BNL [18].

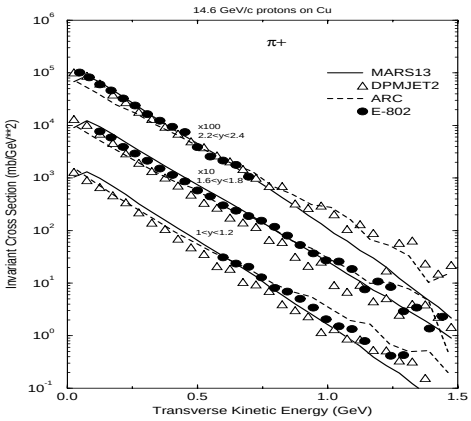

Fig. 1: Production cross sections of π^+ on copper target for 14.6 GeV/c protons.

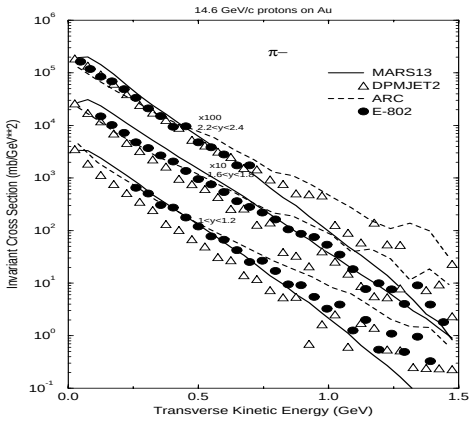

Fig. 2: Production cross sections of π^- on gold target for 14.6 GeV/c protons.

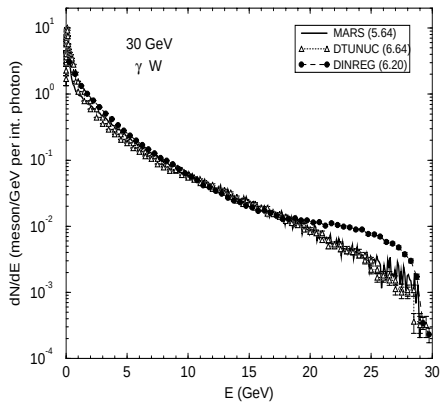

Fig. 3: π+K energy spectrum for 30 GeV photon on tungsten nucleus.

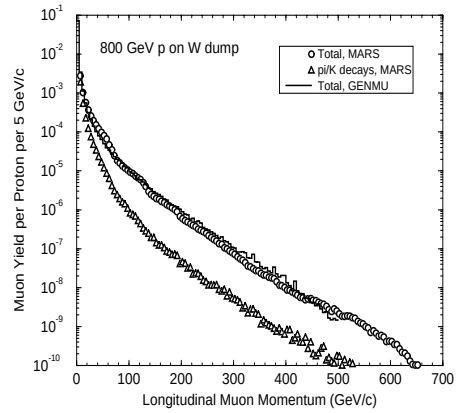

Fig. 4: Muon spectrum after the tungsten absorber for 800 GeV protons.

The π+K energy spectra for 30 GeV photons on tungsten nucleus as calculated with MARS, DTNUC2 [19] and DINREG [20] are presented in Fig. 3. The mean meson multiplicities are shown in the legend. Fig. 4 shows a source term for the τ-neutrino experiment at Fermilab – muon yield from a 1-m long tungsten absorber irradiated with a 800 GeV proton beam. The muon spectrum is dominated by prompt muons and the MARS, and GENMU [21] calculations practically coincide. Fig. 5 illustrates the use of the tagging techniques to calculate a number of muons in the detector components *vs* distance of the primary beam decay from the interaction point in a 2×2 TeV $\mu^+\mu^-$ collider [15]. Partial and total dose equivalent due to neutrino interactions in soil, air, concrete wall and a tissue-equivalent phantom downstream a 2 TeV muon collider straight section is shown in Fig. 6 [6].

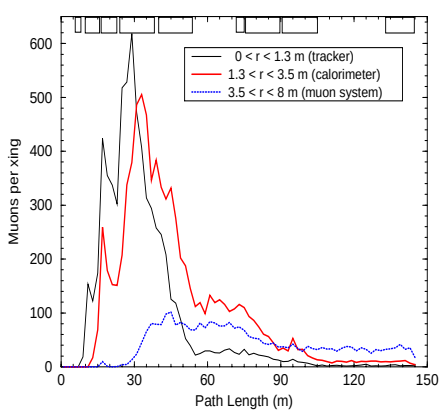

Fig. 5: Background muons at the detector *vs* distance from the IP of 2 TeV μ-decays.

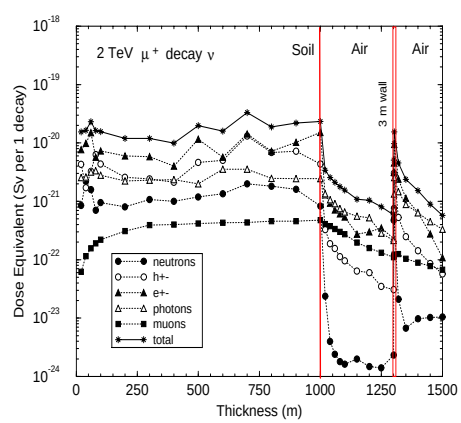

Fig. 6: Dose equivalent due to neutrino from 2 TeV μ^+ decays in soil and air.

4 MARS-MCNP Coupling

Transport of low-energy neutrons (E<14.5 MeV) in MARS13 and earlier versions is based on the 28-group BNAB library [22] in the P_5-approach. In the MARS14 code this module has been replaced with MCNP4A – a general-purpose, continuous-energy, coupled neutron-photon-electron Monte Carlo transport code system [23]. This is an unformal standard in the low-energy domain, representing over 400 person-years of development at the Los Alamos National Laboratory. The MCNP uses pointwise and multigroup cross-section data, mostly based on the latest ENDF/B-VI library in the 10^{-11} to 20 MeV energy range. The cross-section tables in the standard ORNL/RSICC distribution provide data for most existing isotopes and natural mixtures for many elements. Thermal neutrons are described by both the free gas and $S(\alpha, \beta)$ models.

Besides the best coupled physics treatment at E<20 MeV, MCNP offers an extensive use of a few classes of variance reduction techniques which, used correctly, can greatly help the user to produce a more efficient calculation. The non-analog MCNP features fit very well in the MARS philosophy. The MCNP ability to follow target temperature and to provide proper treatment for cells with different temperatures – a rather typical situation at high energy accelerators – is quite essential for low-energy neutron transport. In MARS14, neutron interactions below 20 MeV are treated by the corresponding MCNP modules, while geometry description, source specification, trajectory handling, tally calculations and I/O processing are performed, as for any other particle, by MARS itself. More work is needed to combine MARS and MCNP input files into a single command file, and to exploit the powerful MCNP error analyses for the entire MARS system.

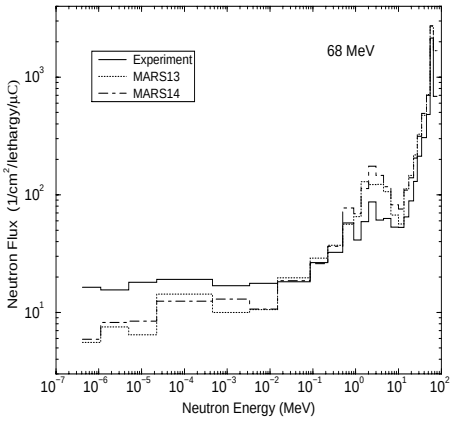

Fig. 7: Transmitted neutron spectra through a 50-cm thick concrete shield for the 68-MeV p-Li neutron source.

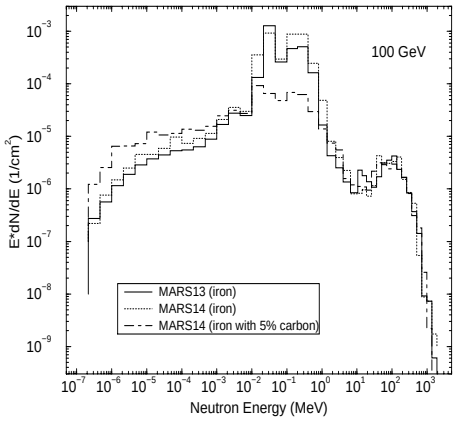

Fig. 8: Neutron energy spectra leaked from the side (R=77 cm) of the iron cylinder irradiated with 100 GeV protons.

A few runs have been performed with MARS14 for incident neutrons at E<20 MeV and perfect agreement has been found in comparison with the original MCNP4A results. Several benchmark runs were done to compare the neutron spectra transmitted through the thick iron and concrete shields for the 43 and 68 MeV p-Li neutron sources. The MARS14 results are rather close to both the experimental data [24] and the MARS13 calculations (see Fig. 7).

The MARS14 results have been compared to those of the other available particle physics codes for an iron cylinder, 300 cm of length and 77 cm of radius, irradiated with 100 GeV protons [1, 25]. The iron with density of ρ=7.4 g/cm^3 contains 5% by weight carbon. The front, side and back leakages of neutrons are scored and presented in Table. The agreement among the different codes is very good. The last two rows in the Table show results calculated with MARS13 and MARS14 for a pure iron cylinder, which are in a good agreement with each other and differ, naturally, from the case of iron with carbon. Fig. 8 shows the neutron spectra leaked from the side of the cylinders made of pure iron and iron with 5% by weight carbon.

Code	% of Carbon	Neutron Leakage		
		Front	Side	Back
LAHET/MCNP	5	102.0	54.4	0.13
GCALOR	5	92.6	64.9	0.19
CALOR89(MORSE)	5	83.9	43.6	0.24
MARS14	5	87.5	52.6	0.16
MARS13	0	150.1	268.1	0.97
MARS14	0	160.4	332.0	1.20

5 MARS-ANSYS Interface

The possibility to calculate an instantaneous temperature rise (with temperature-dependent heat capacity) was built into the previous MARS versions, allowing a thermal analysis for a single pulse. For the current version, the MARS code and the ANSYS 5.1 finite element system [26] have been combined to study thermal and mechanical effects induced by beams in accelerator components. A sophisticated interface has been created to convert the MARS-calculated energy deposition map into the ANSYS input load file [27]. It uses the interpolation and approximation techniques to create the finite element model with contact interface between different cells (materials) for the ANSYS mesh. This makes MARS14 a powerful tool for thermal and stress analyses for a variety of time-dependent beam-induced problems. As an example, Fig. 9 shows calculated temperature as a function of time in the NLC copper target (R=6 mm) irradiated with a 6.22 GeV electron beam (σ_x=σ_y= 1.6 mm) [28]. The equivalent stress map in a copper target (30 cm long, 1 cm radius) at 30 GeV after the first pulse of 5×10^{13} protons is presented in Fig. 10.

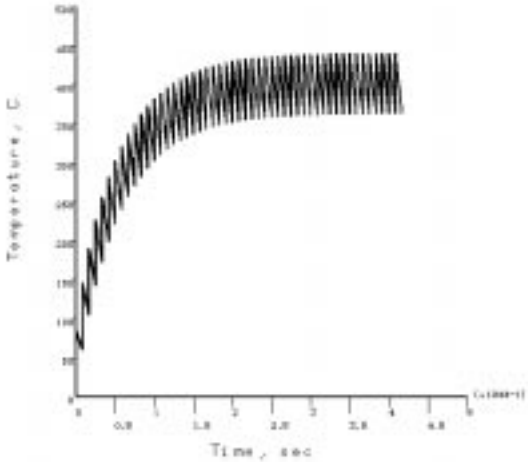

Fig. 9: Time dependence of T_{max} in a copper target irradiated with 6.22 GeV electrons.

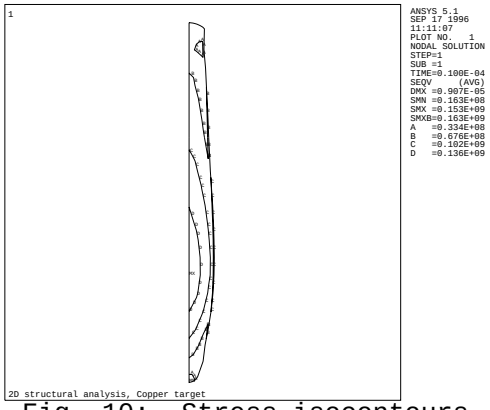

Fig. 10: Stress isocontours (Pa) in a muon collider copper target for a 30 GeV proton beam.

6 OO Geometry Module

The MARS geometry module [1] treats an arbitrary 3-D configuration. It allows an experienced user to describe a shielding, detector or accelerator geometry of almost arbitrary complexity. The main shortcomings are limited visualisation and debugging support, and a limited possibility for an interface to the existing GEANT-like geometry databases. A new geometry module based on the object-oriented engine [13] has been recently embedded into the MARS system. In MARS14 it is integrated with the MARS standard $R - Z - \phi$ geometry module and replaces it's *non-standard* and *extended* geometry parts. The new module is based on the constructive solid geometry representation of the boolean algebra operations on the primitive bodies together with arbitrary rotations and translations. The VRML/2.0 is chosen as the description language – the newly approved standard for a 3-D WWW-oriented geometry description [29]. This allows one to rely on a convenient VRML-enabled WWW browser for a navigation through the entire geometry and a link of the geometry description to the user Web page. The work is in progress to extend the VRML parser/binding and to use the VRML srcipting to represent MARS results. Current MARS option is an OpenGL™-based module [13] – a user-friendly flexible tool to display and handle the studied configuration and particle trajectories (see Fig. 12).

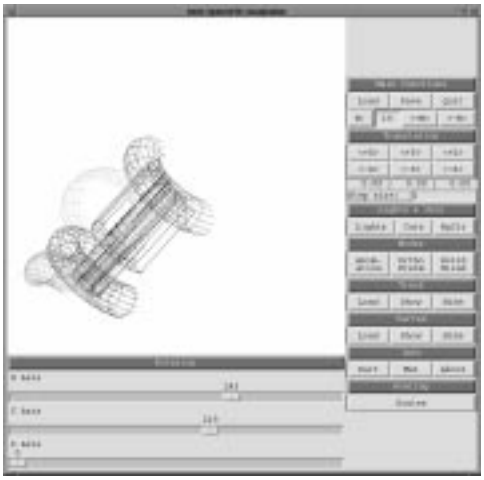

Fig. 11: MARS/OPENGL representation of toroidal geometry.

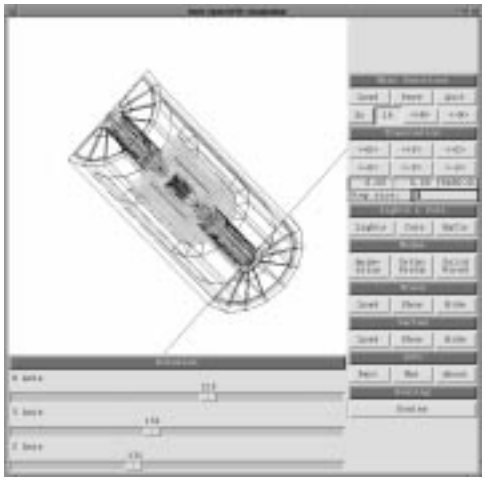

Fig. 12: MARS/OPENGL representation of the CMS detector in the LHC hall.

7 Conclusions

The MARS code possibilities have been substantially extended since the previous official release [1]. Its reliability is confirmed by recent benchmarking described in this paper, in [30], in a comprehensive code verification at the recent SATIF-3 meeting [31], and by several recent applications at Fermilab Tevatron and DØ detector, where MARS predictions have been in excellent agreement with the data. The MARS code unique features allow its successful use in many projects worldwide, such as future Fermilab machine and detector upgrades, numerous studies for high-luminosity 2×2 TeV and 250×250 GeV $\mu^+\mu^-$ colliders, for TESLA and NLC e^+e^- colliders, studies of muons around the LHC machine, optimization of the LHC inner triplets with respect to machine components protection and background minimization in the CMS and ATLAS detectors, studies at the Thomas Jefferson and KEK national laboratories and much more.

References

[1] N. V. Mokhov, "The MARS code system Users Guide, version 13(95)", Fermilab–FN–628, 1995.

[2] V. S. Barashenkov, "Particle and Nucleus Cross-Sections", Dubna, 1993.

[3] N. V. Mokhov and S. I. Striganov, *Beam Dynamics and Technology Issues for $\mu^+\mu^-$ Colliders*, AIP Conference Proceedings **372**, p. 234, Montauk, NY, 1995.

[4] Mokhov, N. V., and Striganov, S. I., "Towards Reliable Prediction of Particle Production for 6-120 GeV Proton Beams", presented at the Workshop on Physics at the First Muon Collider, Fermilab, November 1997.

[5] J. Ranft, *Phys. Rev.*, **D51**, 64, 1995; Gran Sasso report INFN/AE-97/45, 1997.

[6] N. V. Mokhov and A. Van Ginneken, "Muon Collider Neutrino Radiation", in press (1997); presented at Muon Collider Collaboration meeting, Orcas Island, VA, May 1997.

[7] N. V. Mokhov and A. Van Ginneken, to be published.

[8] B. S. Sychev, "Approximation of the differential cross-section of nucleon-nuclei elastic scattering in the energy range above 10 MeV", *Vesti Akademii Nauk BSSR, Seriya Fiziko-energeticheckikh Nauk*, No. 4, Minsk, pp.13-16 (1986).

[9] N. V. Mokhov, "Muons at LHC. Part 1: Beam Dumps", CERN/TIS–RP/TM/95–27, 1995.

[10] Y. Tsai, *Rev. Mod. Phys.* **46**, No. 4, 815–851, 1974.

[11] "Review of Particle Properties", *Phys. Rev.* **D50**, No. 3, 1994.

[12] ICRP Publication 51, "Data for Use in Protection Against External Radiation", Annals of the ICRP 17(2/3), 1987.

[13] O. Krivosheev and N. Mokhov, "OO Geometry Engine for Monte-Carlo Simulation", *Proc. of Radiation Protection and Shielding Topical Meeting*, p. 487, No. Falmouths MA, 1996.

[14] N. V. Mokhov, *Nucl. Phys. B (Proc. Suppl.)*, **51A**, 210, 1996.

[15] C. Johnstone and N. Mokhov, "Optimization of a Muon Collider Interaction Region with Respect to Detector Backgrounds and the Heat Load to the Cryogenic Systems", Fermilab–Conf–96/366, 1996.

[16] A. Drozhdin, M. Huhtinen and N. Mokhov, *Nucl. Instr. and Methods*, **A381**, 531, 1996.

[17] IEEE Standard 754-1985 for Binary Floating-Point Arithmetic, IEEE, 1985.

[18] D. Kahana and Y. Torun, BNL-61983, 1995.

[19] R. Engel, J. Ranft ans S. Roesler, Siegen SI-96-09, SI-96-14, 1996.

[20] P. Degtyarenko and M. Kossov, “Monte-Carlo Program for Nuclear Fragmentation”, Preprint ITEP-11-92, Moscow, 1992.

[21] B. Lundberg, “E-872 Prompt Neutrino Beam”, Fermilab, 1996.

[22] L. P. Abagyan et al., “Group Cross-Sections for Reactor and Shielding Calculations”, Moscow, Energoizdat, 1981.

[23] J. F. Briesmeister, editor, “MCNP - A General Monte Carlo N-Particle Transport Code”. Version 4A. Pub. LA–12625–M, LANL, 1993.

[24] Y. Nakane, K. Hayashi, Y. Sakamoto et al., “Neutron Transmission Benchmark Problems for Iron and Concrete Shields in Low, Intermediate and High Energy Proton Accelerator Facilities”, JAERI-Data/Code 96–029, 1996.

[25] P. K. Job et al., “Neutron Fluence Calculations for the SDC Detector and the Results of Codes Comparison”, *Proc. 8th Int. Conference on Radiation Shielding*, p. 980, Arlington TX, 1994.

[26] Swanson Analysis Systems, *Inc.*,“ANSYS (Revision 5.1)”, SASI/DN-P511:51, Houston, USA, 1994.

[27] N. V. Mokhov and I. V. Novitski, “MARS-ANSYS Coupling for Thermal and Mechanical Analyses of Beam-induced Effects”, to be published.

[28] O. Krivosheev, N. Mokhov and S. Striganov, “NLC Positron Production Target”, Fermilab–TM–1965, 1996.

[29] “The Virtual Reality Modeling Language”, ISO/IEC DIS 14772-1, 1997.

[30] T. Suzuki et al., “Comparison Between Soil Benchmark Experiment and MARS Calculation”, KEK Preprint 97-15, May 1997.

[31] Y. Nakane et al., “Intercomparison of Neutron Transmission Benchmark Analyses for Iron and Concrete Shields in Low, Intermediate and High Energy Proton Accelerator Facilities”, presented at the SATIF-3 meeting, Sendai, Japan, May 1997.